Anonymous Referee #3:

General comments:

This paper investigates whether urban heat islands in a dense metropolitan corridor should be treated as separate local phenomena, or as a connected thermal system linked by urban heat advection. Using five years of station observations and WRF-SLUCM experiments over the Suzhou–Wuxi–Changzhou region, the authors show that heat is transported from upwind to downwind cities, that this effect is much stronger at night than during the day, and that wind speed and boundary-layer depth jointly regulate both the magnitude and even the sign of the advection signal. The paper is interesting because it moves the discussion from single-city UHI toward inter-city thermal coupling, and the combined use of long-term observations and targeted sensitivity tests gives the study a solid basis. At the same time, several aspects of the analysis need to be treated more carefully.

RESPONSE: We sincerely thank you for the time and effort you devoted to reviewing this manuscript. We are grateful for your very positive feedback on our work. We have carefully considered all the constructive comments and revised the manuscript accordingly. Please find our point-by-point responses below.

Specific comments:

1. The paper at times attributes the downstream warming too directly to UHA. In the sensitivity experiment, changing urban land to cropland also changes surface roughness, moisture flux, and local circulation. I suggest the authors use slightly more careful language and clarify that the downstream response cannot be treated as pure advection alone.

RESPONSE: We thank the reviewer for these constructive comments on attributing the downstream response. Indeed, the downstream temperature increase cannot be entirely attributed to UHA. We have enhanced the statement and added a paragraph to discuss the simulation results.

Lines 441—447 of the revised manuscript in Section 3.3:

"In addition, the enhancement of downstream UHI (CUHII and BUHII) is primarily contributed to by UHA, though it is not entirely attributable to this mechanism; it is concurrently modulated by other physical processes. For example, advective transport from upstream urban areas can modify local atmospheric conditions (e.g., ambient humidity, stability), which subsequently influence the thermal environment of the downstream city. Furthermore, changes in the underlying surface will also affect local circulation by thermal (e.g., lake-land breeze circulation) and dynamic (e.g., ventilation) effects, which in turn affect wind and temperature in downstream areas. Ultimately, the increase in downstream UHI is a combined result of multiple processes."

In addition, we added the discussion about changing urban LULC to cropland also changes surface roughness, and the downstream temperature anomaly encompasses both the thermal and dynamic modifications inherent to urbanization.

Lines 353—361 in Section 3.3: "Figure 10 illustrates the spatial distribution of the 2-meter temperature difference between the control and sensitivity simulations (CTRL minus EXP), approximately representing the thermal and dynamic contributions of upstream urbanization in Changzhou to the downstream canopy temperature. During the analysis hours, northwest winds prevailed in domain 3. Influenced by the UHI, Changzhou exhibited a pronounced warming, with positive temperature anomalies of 3.58 °C and 0.42 °C at 22:00 BST and 15:00 BST, respectively. This phenomenon arises from the coupled interplay of thermal and dynamic processes. Thermally, urban materials and anthropogenic heat emissions drive a substantial increase in sensible heat flux. Dynamically, the elevated aerodynamic roughness length of the urban canopy suppresses near-surface wind speeds and ventilation (Oke et al., 2017). Both factors together modulate the local positive temperature anomaly and determine its subsequent advection propagation to downstream regions."

2. The discussion of PBLH may need a more cautious interpretation. The observational PBLH product is relatively coarse, and the model also has known uncertainty in wind speed and PBLH. Since PBLH is central to the main argument, the related uncertainty should be acknowledged more clearly.

RESPONSE: We are grateful for the reviewer's call for a more cautious treatment of the PBLH uncertainty. Different data sources, such as ceilometer lidar, satellite, radiosonde, and reanalysis datasets, can reach quite different estimates of PBLH (Saha et al., 2022). ERA5 is the most promising reanalysis data source in terms of characterizing the evolution of PBLH, with an underestimation of daytime PBLH of around 130 m when compared to high-resolution radiosonde (Guo et al., 2021). The dataset (A merged continental planetary boundary layer height dataset based on high-resolution radiosonde measurements, ERA5 reanalysis, and GLDAS) uses machine learning to correct systematic biases in the ERA5 reanalysis data (Guo et al., 2024). Therefore, we use this dataset to represent regional PBLH, and we have supplemented the uncertainty of this dataset as follows:

Lines 123—125 of the revised manuscript in Section 2.1:

"The mean bias between the dataset and the PBLH recovered from radiosonde observations is −0.9 m, and the root mean square error (RMSE) of the training set and the test set is 243 m and 370 m,

respectively."

We added comparisons of the RMSE and mean bias (MB) between WRF and the PBLH dataset. Compared to the dataset, the PBLH obtained from the WRF is lower during the day and higher at night.

Lines 323—331 of the revised manuscript in Section 3.3:

"In addition, the RMSE of PBLH between the model and the dataset (Guo et al., 2024) is 262 m. … For the PBLH, the MB compared to the radiosonde-reanalysis merged dataset was –66 m."

In addition, we further validated the simulated wind speed and direction (Fig. R1). The RMSE for wind direction was 35.86°, which reasonably reproduced the wind direction. The RMSE for wind speed was 4.68 m s^{-1}, R = 0.64 ($p < 0.001$), which is due to the SLUCM systematically overestimating near-surface wind speed (Avisar et al., 2021; Sun et al., 2021; Yu et al., 2021). Therefore, we replaced SLUCM with MLUCM (BEP+BEM) and coupled a global 1 km spatially continuous urban canopy parameter for the WRF model (Liao et al., 2025). Furthermore, to meet the configuration requirements of BEM, the PBL scheme was replaced by MYJ instead of YSU. The results show that the improved BEP effectively improves the wind speed overestimation (Fig. 8).

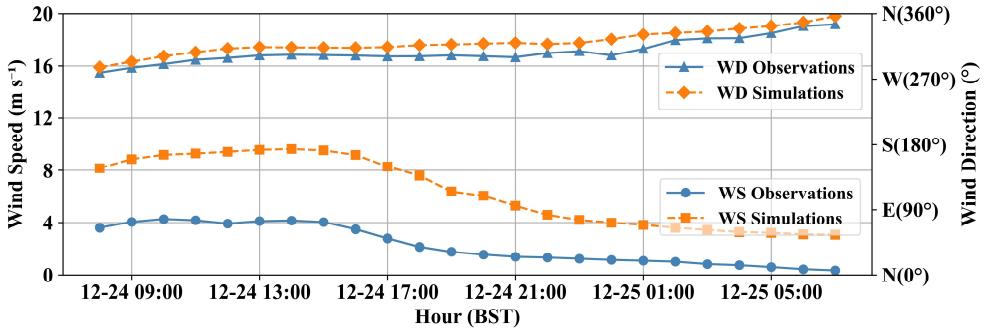

Figure R1. Comparisons of hourly mean 10-meter wind speed (below lines) and wind direction (above lines) from WRF simulations and observations within the ROI.

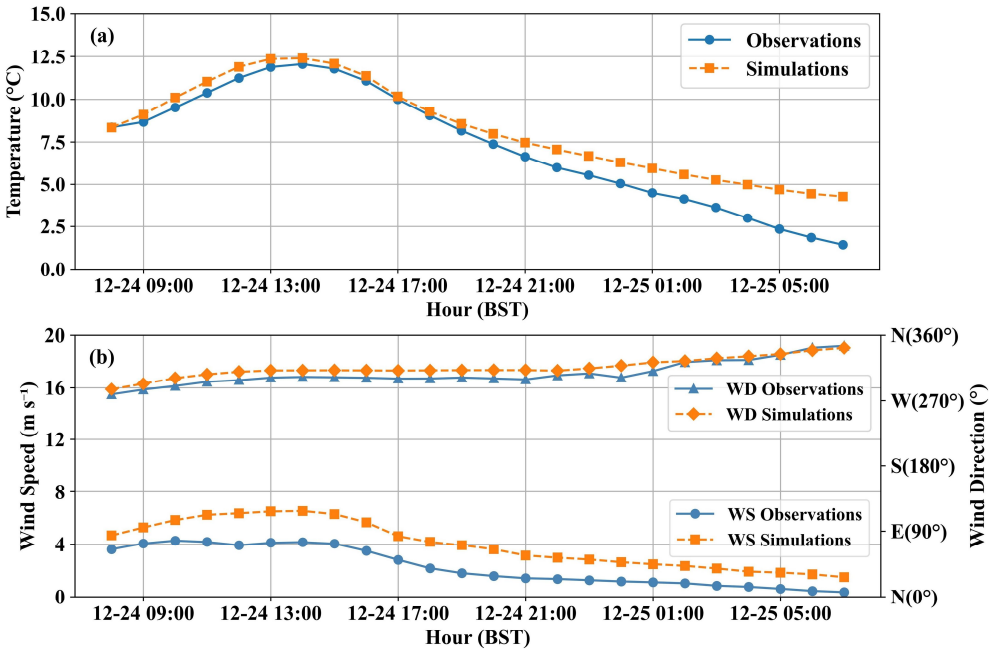

Figure 8. Comparisons of hourly mean (a) 2-meter temperature and (b) 10-meter wind speed (below lines) and wind direction (above lines) from WRF simulations (orange lines) and observations (blue lines) within the ROI.

Line 320—333 in Section 3.3:

"Model performance was evaluated by comparing simulated 2-m air temperature and 10-m wind field of domain 3 against hourly observations from all available meteorological stations within the ROI (Fig. 8). For 2-m air temperature, the RMSE and the Pearson correlation coefficient (R) were 1.80 °C and 0.92 ($p < 0.001$), respectively (Fig 8a). For 10-m wind field, the RMSE for wind direction and wind speed were 34.77° and 2.62 m s^{-1}, respectively (Fig 8b). In addition, the RMSE of PBLH between the model and the dataset (Guo et al., 2024) is 262 m. To provide a more comprehensive validation of the model's performance, we calculated additional statistical metrics for the simulation period. For 2-m air temperature, the Mean Absolute Error (MAE) was 1.29 °C, the Mean Bias (MB) was 0.99 °C (indicating a slight warm bias), and the Index of Agreement (IOA) was 0.93. For 10-m wind speed, the MAE was 2.01 m s^{-1} and the MB was +1.70 m s^{-1} (reflecting a typical overestimation of wind speed by WRF in urban areas due to simplified canopy drag representations (Yu et al., 2021)), with an IOA of 0.71. For the PBLH, the MB compared to the radiosonde-reanalysis merged dataset was –66 m. These quantitative metrics demonstrate that the model captures both the diurnal thermal cycle and the wind-driven transport dynamics with acceptable accuracy, establishing a solid baseline for the sensitivity experiments."

Furthermore, Section 3.3 has been comprehensively revised based on the new simulation results. Please refer to the end of this response for details.

3. The observational UHA index is useful, but it is still a statistical proxy rather than a direct physical estimate of heat advection. It would strengthen the paper if the authors explain this point more clearly, and, if possible, compare it briefly with the advection term from the WRF results. A simple validation of the model wind field would also help.

RESPONSE: We appreciate this suggestion to compare the observational index with the model advection term and to validate the wind field. We have compared the UHA intensity with the horizontal temperature advection term based on the WRF model as follows:

Lines 183—186 of the revised manuscript in Section 2.2.3:

"In addition, the horizontal temperature advection term in the thermodynamic energy equation was calculated as follows:

$$A_T = -(U\frac{\mathrm{dT}}{\mathrm{dx}} + V\frac{\mathrm{dT}}{\mathrm{dy}}), \quad (4)$$

where U and V are the horizontal wind components, and T is the air temperature. All variables were taken from the lowest atmospheric layer of the model."

Lines 339—351 of the revised manuscript in Section 3.3:

"The observation-based UHA intensity was compared with the WRF-simulated horizontal temperature advection. Taking Wuxi (U4), which lies downwind of Changzhou (U2) under the prevailing northwest wind direction, as an example, the observed daily mean CUHII during the simulation period was 2.24 °C (Fig. 9a). The UHA intensity was negative after sunrise, turned positive around midday, and continued to intensify, reaching a maximum of 3.15 °C at night before declining toward the following morning (Fig. 9b). The daily mean UHA intensity was 1.38 °C, indicating that UHA enhances CUHII under the prevailing wind direction. Fig. 9c shows the difference in horizontal temperature advection between the control and sensitivity experiments (CTRL minus EXP). This difference also exhibited a broadly similar pattern with higher values at night and lower values during the day, with a nighttime peak of approximately 0.45 K/h and a daily mean of 0.18 K/h (Fig. 9c). Overall, the UHA intensity and the horizontal temperature advection showed similar diurnal variations."

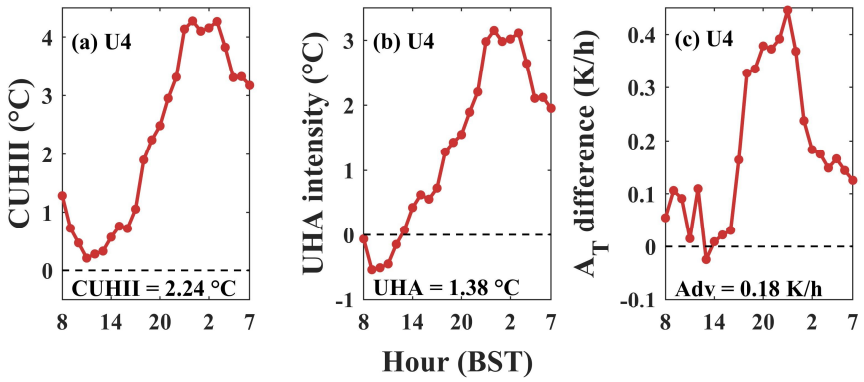

Figure 9. Diurnal variation of hourly (a) CUHII, (b) UHA intensity, and (c) horizontal temperature advection difference between the control simulation and the sensitivity experiment (CTRL minus EXP) over Wuxi (U4) during the simulation period. Annotated values indicate the respective daily means.

Furthermore, we have added validations of wind speed and direction as stated in RESPONSE 2 above.

4. The BUHI calculation needs a little more methodological clarification. The current method appears to use a arithmetic mean, while the WRF vertical levels are unevenly spaced. This may give too much weight to the near-surface layers. The authors may clarify whether a thickness-weighted or mass-weighted average would be more appropriate, or note the possible sensitivity.

RESPONSE: We thank the reviewer for raising the issue of vertical averaging across non-uniform levels. We have revised this issue by using the thickness-weighted average (by introducing the height of the vertically staggered grid) to ensure an accurate representation of the boundary layer.

Lines 191—202 of the revised manuscript in Section 2.2.4:

$$BUHII_i(t) = \langle\theta_i\rangle_{\mathrm{PBL}} - \langle\theta_r\rangle_{\mathrm{PBL}}, \quad (6)$$

where $\langle\theta_i\rangle_{\mathrm{PBL}}$ and $\langle\theta_r\rangle_{\mathrm{PBL}}$ represent the thickness-weighted average potential temperature within the boundary layer over urban and rural areas, respectively. Taking the urban area as an example:

$$\langle\theta_i\rangle_{\mathrm{PBL}} = \frac{1}{N_i}\sum_{j=1}^{N_i}\frac{\sum_{k=1}^{K_{i,j}}\theta_{i,j,k}(t)\Delta z_{i,j,k}}{\sum_{k=1}^{K_{i,j}}\Delta z_{i,j,k}}, \quad (7)$$

$$\Delta z_{i,j,k} = zstag_{i,j}(k+1) - zstag_{i,j}(k), \quad (8)$$

where N_i is the number of grid points in the urban region i; for a given grid point j, $K_{i,j}$ denotes the number of vertical layers from the lowest model level to the PBLH (output by the model); and $\theta_{i,j,k}(t)$ is the potential temperature at time t at the k-th layer of grid point j. $\Delta z_{i,j,k}$ denotes

the physical thickness of the k-th vertical layer, and $zstag$ denotes the height of vertically staggered grid. The calculation method for the rural area $\langle\theta_r\rangle_{\mathrm{PBL}}$ is similar:

$$\langle\theta_r\rangle_{\mathrm{PBL}} = \frac{1}{N_r}\sum_{j=1}^{N_r}\frac{\sum_{k=1}^{K_{r,j}}\theta_{r,j,k}(t)\Delta z_{r,j,k}}{\sum_{k=1}^{K_{r,j}}\Delta z_{r,j,k}}, \quad (9)$$

The result of SLUCM is as follows:

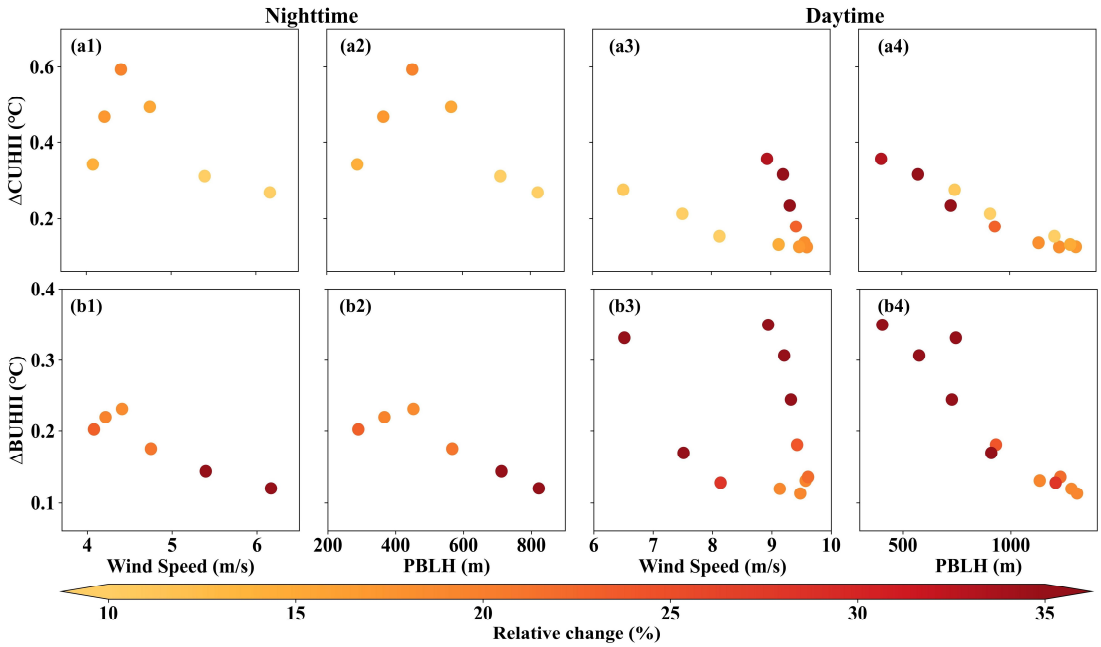

Figure R4. Scatter plots between ΔCUHII and (a1, a3) 10-meter wind speed, and (a2, a4) PBLH between the control simulation and the sensitivity experiment (CTRL minus EXP) at (a1-a2) nighttime and (a3-a4) daytime. (b1-b4) Same as (a1-a4), but for ΔBUHII. Colours represent the relative change of CUHII or BUHII. Note that only the moment when the northwest wind prevailed in the ROI was reserved.

The result of MLUCM (BEP+BEM) in section 3.3 is as follows:

Lines 425—430 of the revised manuscript in the Section 3.3:

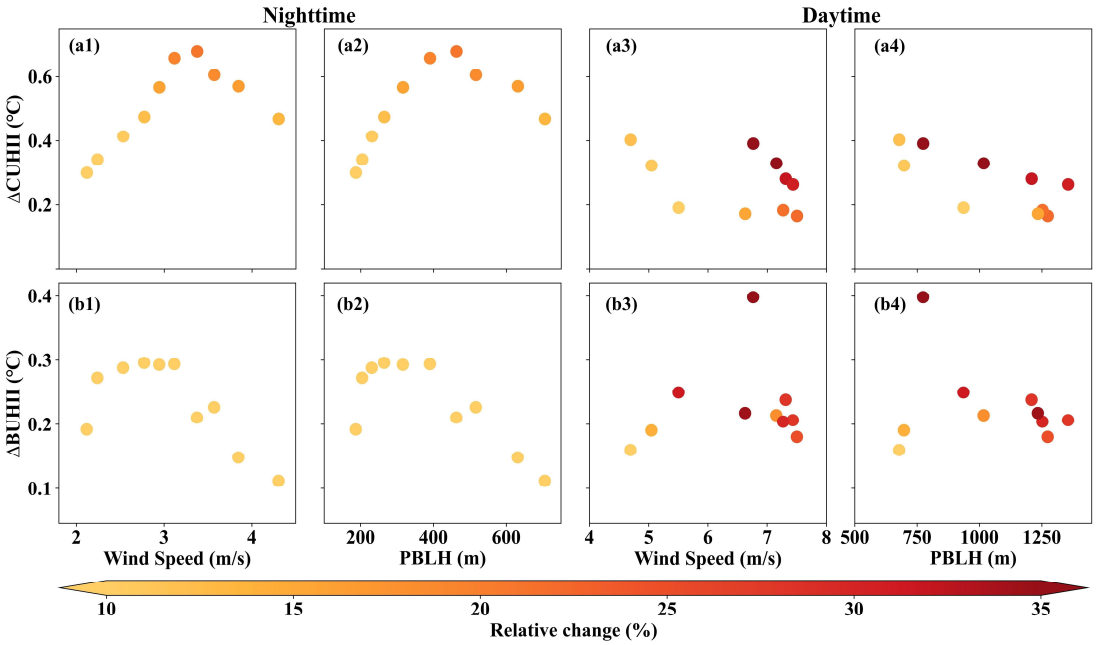

Figure 12. Scatter plots between ΔCUHII and (a1, a3) 10-meter wind speed, and (a2, a4) PBLH between the control simulation and the sensitivity experiment (CTRL minus EXP) over Wuxi (U4) at (a1-a2) nighttime and (a3-a4) daytime. (b1-b4) Same as (a1-a4), but for ΔBUHII. Colours represent the relative change of CUHII or BUHII. Note that only the moment when the northwest wind prevailed in the ROI was reserved.

For ΔCUHII, the results obtained from the two schemes are consistent, and they are consistent with the conclusions from observation. For ΔBUHII, the absolute magnitude is comparable between SLUCM (YSU) and BEP+BEM (MYJ), but the response to daytime wind speed and PBLH differs between the two schemes. Due to the lack of temperature observation data above the PBL, this study focuses on the magnitude of ΔBUHII variation and does not explore its relationship with wind speed and PBLH. Furthermore, we have added a discussion about the uncertainties of ΔBUHII in the results due to different schemes of PBL and urban models.

Lines 406—440 of the revised manuscript in Section 3.3:

"The CUHII differences of the downstream adjacent city Wuxi (U4) were evaluated between two experimental scenarios. Figures 12a–d show scatter plots of ΔCUHII and both wind speed and PBLH across different hours. Nighttime conditions exhibited a higher ΔCUHII (with a maximum increase of 0.68°C), accompanied by lower wind speed and shallower PBLH (Fig. 12a1–a2); while daytime conditions showed a comparatively lower ΔCUHII (with a minimum increase of 0.17°C), accompanied by higher wind speed and deeper PBLH (Fig. 12a3–a4). The relative increase in CUHII ranged from 8.1% to 60.4%, with the large proportional amplifications occurring during the

daytime period. Specifically, the average difference between nighttime and daytime is 0.51 °C (14.2%) and 0.27 °C (18.9%), respectively. At night, ΔCUHII exhibited a non-linear response to increases in wind speed and PBLH, characterized by an initial amplification followed by a decrease (Fig. 12a1–a2). In contrast, daytime ΔCUHII decreased with increasing PBLH, while its correlation with wind speed remained ambiguous (Fig. 12a3–a4). In summary, these sensitivity experiments provide corroborations for the observational findings, confirming that UHA is regulated by wind speed and PBLH non-linearly.

UHA also contributed to an increase in BUHII in the downstream city of Wuxi (U4, Fig. 12b1–b4). Specifically, ΔBUHII increased by a maximum of 0.40°C and a minimum of 0.11°C, ranging from 4.7% to 41.7%. The average difference between nighttime and daytime is 0.23 °C (7.5%) and 0.23 °C (23.3%), respectively. It should be noted that uncertainties remain in BUHII due to the schemes of PBL and urban canopy (Zhu and Ooka, 2023). In a supplementary sensitivity test utilizing the YSU PBL scheme (Hong et al., 2006) coupled with the SLUCM urban scheme (Fig. S6), while the absolute change in ΔBUHII remains comparable in magnitude, the relative change of ΔBUHII is larger, and its variation characteristics in response to wind speed and PBLH remain uncertain. Because the numerical simulation covered a limited time period, the potential moderating roles of wind speed and PBLH on BUHI were not further examined."

5. Some parts of the physical interpretation may be presented more clearly. The discussion of CUHI, BUHI, and UHA is sometimes mixed together, so the mechanism is not always easy to follow. It would also help to briefly clarify the station classification and rural reference choice, and to note the possible influence of other regional factors such as surface effects, southeast marine air, aerosols, and anthropogenic heat assumptions in the model.

RESPONSE: We thank the reviewer for these suggestions on sharpening the physical interpretation. First, we have revised the discussion of CUHI, BUHI, and UHA as follows:

Lines 454—472 of the revised manuscript in the Discussions:

"When background winds are present, UHA propagates heat downstream and strengthens downstream CUHI and BUHI. Particularly with urban agglomeration development and decreasing inter-city distances, spatial clustering of heat sources amplifies regional thermal risks.

Based on observations and numerical simulations, Figure 13 presents a conceptual diagram of UHA impacts on downwind UHI in the YRD urban agglomeration. Under nocturnal SBL conditions, UHA is confined to a relatively low vertical extent (Cosgrove and Berkelhammer, 2018), with substantial heat propagating downstream primarily within the near-surface layer (orange arrow in

Fig. 13). Under these conditions, the amplification of downstream CUHII is greater than that of BUHII. Vertical mixing of shallow PBL and weak turbulence is detrimental to the cooling of the built-up area environment (Haeffelin et al., 2024). Under daytime CBL conditions, buoyancy-driven turbulence is vigorous, UHA impacts can extend throughout the entire PBL depth (Fig. 11c). As urban thermal plumes are transported downstream over long distances within the PBL, they can be vertically mixed with the lower-level air of downstream cities through turbulence (above the downstream city in Fig. 13). Ultimately, thermal plumes from successive cities coalesce and facilitate further heat transport (Fig. 13).

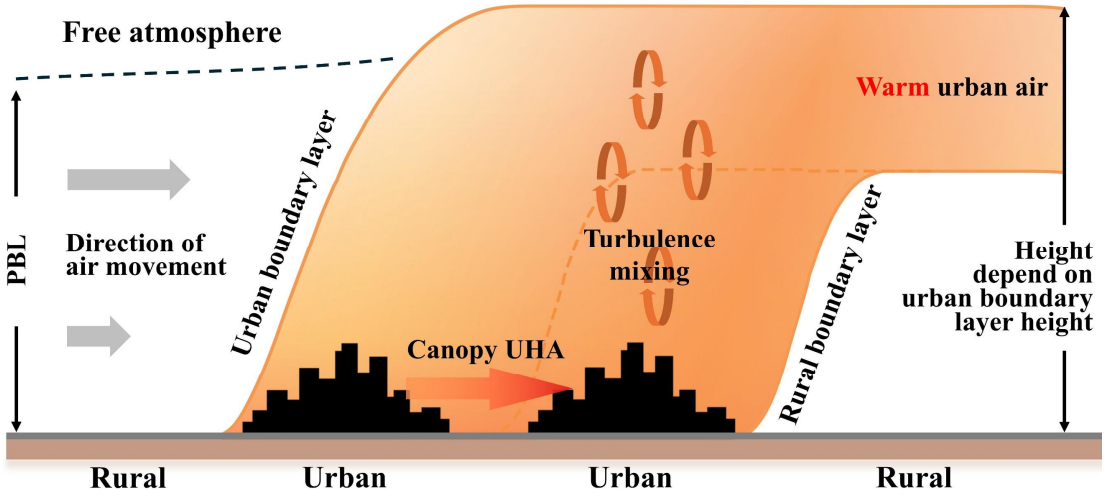

Figure 13. Conceptual diagram showing the impact of UHA on downstream UHI within the Yangtze River Delta urban agglomeration. Modified from Oke (1976) and Cosgrove and Berkelhammer (2018).

Secondly, we further clarified the selection criteria for urban reference stations, and the impact of selecting rural reference stations at different longitudes is limited.

Lines 107—111 of the revised manuscript in Section 2.1:

"Specifically, urban stations (U1–U10) are characterized by densely built-up areas with high AHF intensity (> 5 W/m² in a four-kilometer buffer zone); whereas rural reference stations were matched according to the same latitudinal zone as the urban areas, featuring low impervious surface coverage and flat topography. Sensitivity tests using alternative rural reference stations located closer to the coast suggest that the potential bias arising from the limited longitudinal spread of the rural stations is small."

Third, we have supplemented the possible influence of surface effects as stated in RESPONSE 1 above.

Fourth, we added a discussion of the cooling effect of the southeast sea breeze on the upstream UHA in Section 3.1.

Lines 256—258 in Section 3.1: "Northwest winds mainly exacerbate the CUHI across most regions of the study area, whereas southeast winds exert a more extensive mitigating influence due to the cooling effect of sea breezes (Yang et al., 2023)"

Fifth, in the Section discussion, we explained that the potential impact of aerosols is worth further exploring.

Lines 474—477 in Section 4: "Additionally, downstream cities receive not only heat but also aerosol inputs from upwind urban sources (Baklanov et al., 2016). These aerosols may modulate the CUHII of downstream cities through radiative forcing (Wang et al., 2020; Xue et al., 2023; Yang et al., 2020), and this feedback process warrants further investigation."

Finally, the model AHF from buildings in this study is dynamically calculated by BEM. Using the default BEM thermodynamic equations, the model dynamically computes the real-time energy required for indoor space heating and the subsequent waste heat rejected into the urban atmosphere. This calculation is driven by the instantaneous outdoor meteorological conditions (e.g., ambient temperature, radiation) and building interior target temperatures. We have revised the description of AHF:

Lines 149—155 of the revised manuscript in Section 2.2.3:

"The spatial features of UHA were evaluated using the Weather Research and Forecasting (WRF) model, version 3.9.1, coupled with a multi-layer urban canopy model (MLUCM). This study utilizes the multi-layer Building Effect Parameterization (BEP) coupled with the Building Energy Model (BEM), and urban canopy parameters were taken from the global 1 km spatially continuous GloUCP dataset (Liao et al., 2025). BEP+BEM can reproduce the intensity and spatiotemporal distribution of UHI (Zhu and Ooka, 2023), and it includes a mature parameterization of the air-conditioning system and of indoor–outdoor heat exchange and accounts for the vertical distribution of AHF (Salamanca et al., 2010)"

The original SLUCM run used a default sensible AHF of 50 W m^{-2} scaled by the 24-hour multiplication factors: 0.16 0.13 0.08 0.07 0.08 0.26 0.67 0.99 0.89 0.79 0.74 0.73 0.75 0.76 0.82 0.90 1.00 0.95 0.68 0.61 0.53 0.35 0.21 0.18 (starting at 01 hours local time, no latent AHF).

Furthermore, for numerical simulation, we replaced SLUCM with the MLUCM (BEP+BEM) scheme, drove the urban morphology with the 1 km GloUCP dataset (Liao et al., 2025), and switched the PBL scheme from YSU to MYJ as required by BEM. The entire section 3.3 has been modified based on the new simulation results (as described in RESPONSE 2). Note that the MYJ scheme results show the phenomenon of heat anomalies reaching the top of the PBL

later than YSU, so the displayed times were adjusted. The new results do not affect existing conclusions, and the abstract, data, and methods sections have been modified accordingly.

Line 320—447 in Section 3.3:

"Model performance was evaluated by comparing simulated 2-m air temperature and 10-m wind field of domain 3 against hourly observations from all available meteorological stations within the ROI (Fig. 8). For 2-m air temperature, the RMSE and the Pearson correlation coefficient (R) were 1.80 °C and 0.92 ($p < 0.001$), respectively (Fig 8a). For 10-m wind field, the RMSE for wind direction and wind speed were 34.77° and 2.62 m s^{-1}, respectively (Fig 8b). In addition, the RMSE of PBLH between the model and the dataset (Guo et al., 2024) is 262 m. To provide a more comprehensive validation of the model's performance, we calculated additional statistical metrics for the simulation period. For 2-m air temperature, the Mean Absolute Error (MAE) was 1.29 °C, the Mean Bias (MB) was 0.99 °C (indicating a slight warm bias), and the Index of Agreement (IOA) was 0.93. For 10-m wind speed, the MAE was 2.01 m s^{-1} and the MB was +1.70 m s^{-1} (reflecting a typical overestimation of wind speed by WRF in urban areas due to simplified canopy drag representations (Yu et al., 2021)), with an IOA of 0.71. For the PBLH, the MB compared to the radiosonde-reanalysis merged dataset was –66 m. These quantitative metrics demonstrate that the model captures both the diurnal thermal cycle and the wind-driven transport dynamics with acceptable accuracy, establishing a solid baseline for the sensitivity experiments.

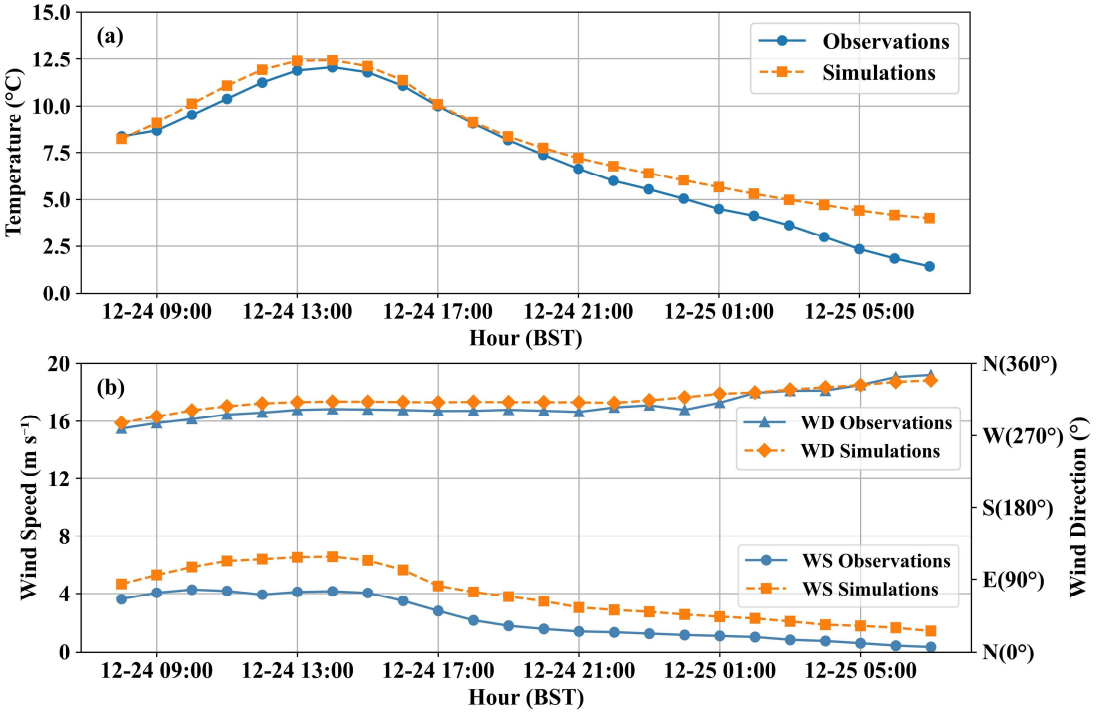

Figure 8. Comparisons of hourly mean (a) 2-meter temperature and (b) 10-meter wind speed (below lines) and wind direction (above lines) from WRF simulations (orange lines) and observations (blue

lines) within the ROI.

The observation-based UHA intensity was compared with the WRF-simulated horizontal temperature advection. Taking Wuxi (U4), which lies downwind of Changzhou (U2) under the prevailing northwest wind direction, as an example, the observed daily mean CUHII during the simulation period was 2.24 °C (Fig. 9a). The UHA intensity was negative after sunrise, turned positive around midday, and continued to intensify, reaching a maximum of 3.15 °C at night before declining toward the following morning (Fig. 9b). The daily mean UHA intensity was 1.38 °C, indicating that UHA enhances CUHII under the prevailing wind direction. Fig. 9c shows the difference in horizontal temperature advection between the control and sensitivity experiments (CTRL minus EXP). This difference also exhibited a broadly similar pattern with higher values at night and lower values during the day, with a nighttime peak of approximately 0.45 K/h and a daily mean of 0.18 K/h (Fig. 9c). Overall, the UHA intensity and the horizontal temperature advection showed similar diurnal variations.

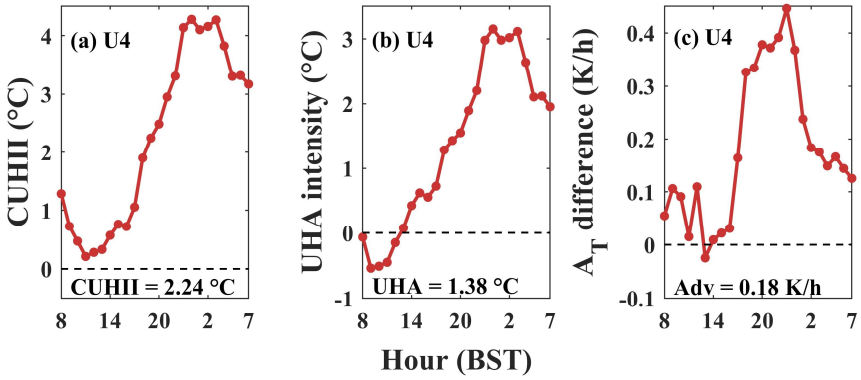

Figure 9. Diurnal variation of hourly (a) CUHII, (b) UHA intensity, and (c) horizontal temperature advection difference between the control simulation and the sensitivity experiment (CTRL minus EXP) over Wuxi (U4) during the simulation period. Annotated values indicate the respective daily means.

"Figure 10 illustrates the spatial distribution of the 2-meter temperature difference between the control and sensitivity simulations (CTRL minus EXP), approximately representing the thermal and dynamic contributions of upstream urbanization in Changzhou to the downstream canopy temperature. During the analysis hours, northwest winds prevailed in domain 3. Influenced by the UHI, Changzhou exhibited a pronounced warming, with positive temperature anomalies of 3.58 °C and 0.42 °C at 22:00 BST and 15:00 BST, respectively. This phenomenon arises from the coupled interplay of thermal and dynamic processes. Thermally, urban materials and anthropogenic heat

emissions drive a substantial increase in sensible heat flux. Dynamically, the elevated aerodynamic roughness length of the urban canopy suppresses near-surface wind speeds and ventilation (Oke et al., 2017). Both factors together modulate the local positive temperature anomaly and determine its subsequent advection propagation to downstream regions. The simulations show a diurnal variation in the 2-meter temperature differences. At night (22:00 BST), lower wind speeds were accompanied by a high UHA intensity but with a limited advective distance, and strong warming was concentrated in the short distance downstream of the city (Fig. 10a). In contrast, daytime conditions (15:00 BST) featured higher wind speeds, which were accompanied by lower UHA intensity but a greater thermal influence distance (Fig. 10b). Under the prevailing northwest winds, the U10 region was also affected by the thermal forcing of Taihu Lake in addition to UHA. During winter, Taihu Lake functions as a daytime heat sink and a nighttime heat source relative to the surrounding environment (Fig. S3). Furthermore, Cosgrove and Berkelhammer (2018) utilized a Lagrangian atmospheric transport model to demonstrate that the Chicago urban thermal plume caused significant heating at 100–200 m above ground level, extending up to 70 km downwind. The sensitivity experiments in this study show that the downstream canopy region was also heated, with the thermal influence beyond 100 km.

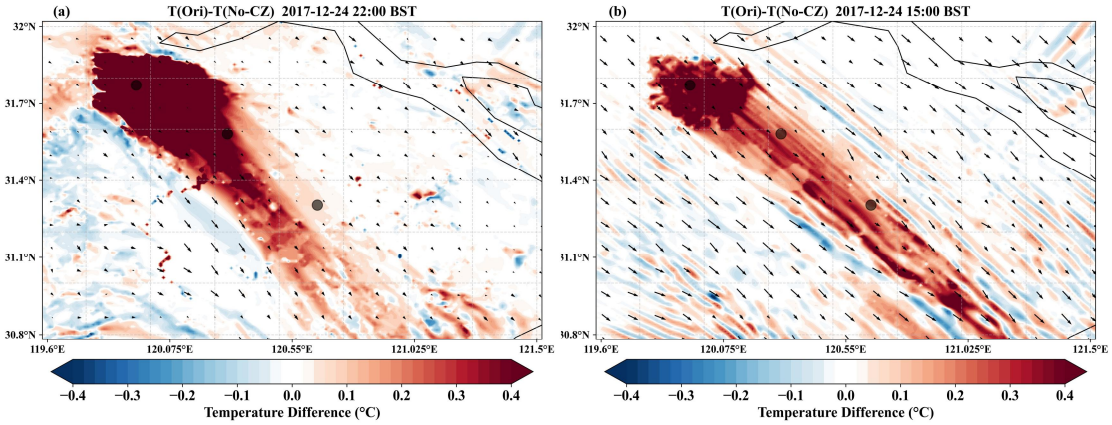

Figure 10. Spatial distribution of the 2-meter temperature difference between the control simulation and the sensitivity experiment (CTRL minus EXP) at (a) 22:00 BST and (b) 15:00 BST. Vector arrows indicate the 10-meter wind field of the CTRL. The three marked locations from northwest to southeast correspond to downtown areas of Changzhou (U2), Wuxi (U4), and Suzhou (U6), respectively.

Vertical cross-sections of potential temperature and wind vector differences between control and sensitivity experiments were analysed (Fig. 11). The cross-section along a northwest-southeast direction spans approximately 114 km (Fig. 11a), encompassing cities from Changzhou (U2) through Wuxi (U4) to Suzhou (U6). Note that the coordinate rotation was applied to the horizontal

wind component u to align it with the cross-section direction, with positive values corresponding to northwest winds. For example, significant negative horizontal wind components within Changzhou's near-surface layer are due to the urban rough surface. At night (22:00 BST), the atmospheric stratification is stable, and updrafts and downdrafts induced by the UHI can be observed over urban areas, particularly in Wuxi (see the CTRL results in Figure S4b). Thermal plume was suppressed within the near-surface layer, and substantial heat within Changzhou propagated downstream primarily below 100 m, although the PBLH can reach 750 m (Fig. 11b). Following sunrise, solar shortwave radiation enhanced surface heating and buoyancy-driven turbulence (Zhang et al., 2023), elevating PBLH to approximately 1600 m by afternoon (15:00 BST, Fig. S4c). Compared to nighttime conditions, enhanced ventilation and vertical mixing extended thermal influences throughout the entire PBL depth (Fig. 11c), intensifying the BUHI in Wuxi and Suzhou. As the thermal plume propagates, vertical heat redistribution may occur through turbulent mixing in downstream cities. In addition, the updraft in the downstream area is strengthened, and the vertical circulation in Wuxi during the day may be UHA-enhanced UHI circulation (Fig. 11b-c).

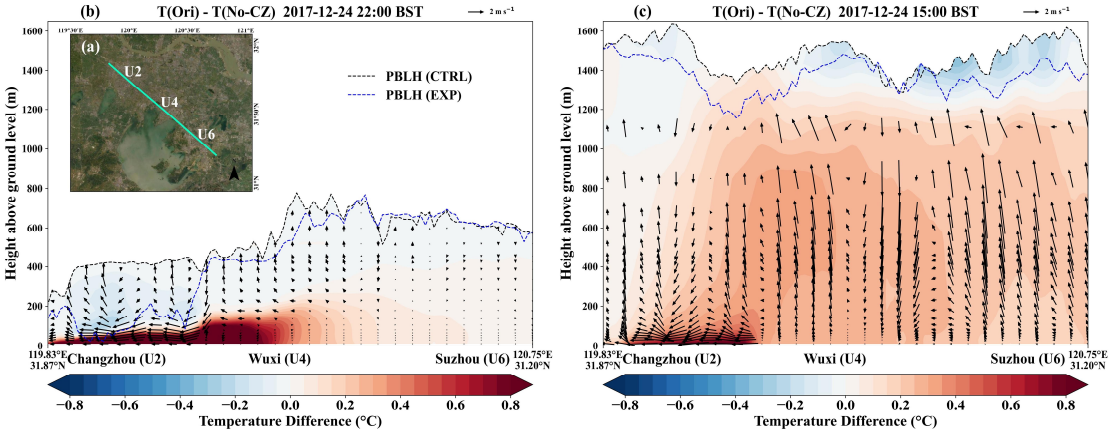

Figure 11. (a) Geographical location of the vertical cross-section. (b, c) Vertical cross-sections of the potential temperature and wind vector differences between the control simulation and the sensitivity experiment (CTRL minus EXP) at (b) 22:00 BST and (c) 15:00 BST. Wind vectors were synthesized by rotating u (along the transect axis) and scaling ω (ω multiplied by 50). The black and blue solid lines denote the PBLH in the CTRL and EXP simulations, respectively.

The sensitivity experiments quantified UHA contributions from a single upstream city. In reality, taking the downstream city of Suzhou as an example, its UHI is influenced by multiple upstream heat sources, including weak UHA transport from distant Changzhou superimposed upon strong UHA contributions from adjacent Wuxi. When the LULCs in upstream Changzhou and Wuxi are simultaneously replaced with croplands in the sensitivity experiment, enhanced cross-city thermal plume superposition and greater PBLH differences were shown (Fig. S5). These results

demonstrate that the intensity and spatial structure of UHA are closely related to diurnal boundary layer evolution.

The CUHII differences of the downstream adjacent city Wuxi (U4) were evaluated between two experimental scenarios. Figures 12a show scatter plots of ΔCUHII and both wind speed and PBLH across different hours. Nighttime conditions exhibited a higher ΔCUHII (with a maximum increase of 0.68°C), accompanied by lower wind speed and shallower PBLH (Fig. 12a1–a2); while daytime conditions showed a comparatively lower ΔCUHII (with a minimum increase of 0.17°C), accompanied by higher wind speed and deeper PBLH (Fig. 12a3–a4). The relative increase in CUHII ranged from 8.1% to 60.4%, with the large proportional amplifications occurring during the daytime period. Specifically, the average difference between nighttime and daytime is 0.51 °C (14.2%) and 0.27 °C (18.9%), respectively. At night, ΔCUHII exhibited a non-linear response to increases in wind speed and PBLH, characterized by an initial amplification followed by a decrease (Fig. 12a1–a2). In contrast, daytime ΔCUHII decreased with increasing PBLH, while its correlation with wind speed remained ambiguous (Fig. 12a3–a4). In summary, these sensitivity experiments provide corroborations for the observational findings, confirming that UHA is regulated by wind speed and PBLH non-linearly.

UHA also contributed to an increase in BUHII in the downstream city of Wuxi (U4, Fig. 12b1–b4). Specifically, ΔBUHII increased by a maximum of 0.40°C and a minimum of 0.11°C, ranging from 4.7% to 41.7%. The average difference between nighttime and daytime is 0.23 °C (7.5%) and 0.23 °C (23.3%), respectively. It should be noted that uncertainties remain in BUHII due to the schemes of PBL and urban canopy (Zhu and Ooka, 2023). In a supplementary sensitivity test utilizing the YSU PBL scheme (Hong et al., 2006) coupled with the SLUCM urban scheme (Fig. S6), while the absolute change in ΔBUHII remains comparable in magnitude, the relative change of ΔBUHII is larger, and its variation characteristics in response to wind speed and PBLH remain uncertain. Because the numerical simulation covered a limited time period, the potential moderating roles of wind speed and PBLH on BUHI were not further examined.

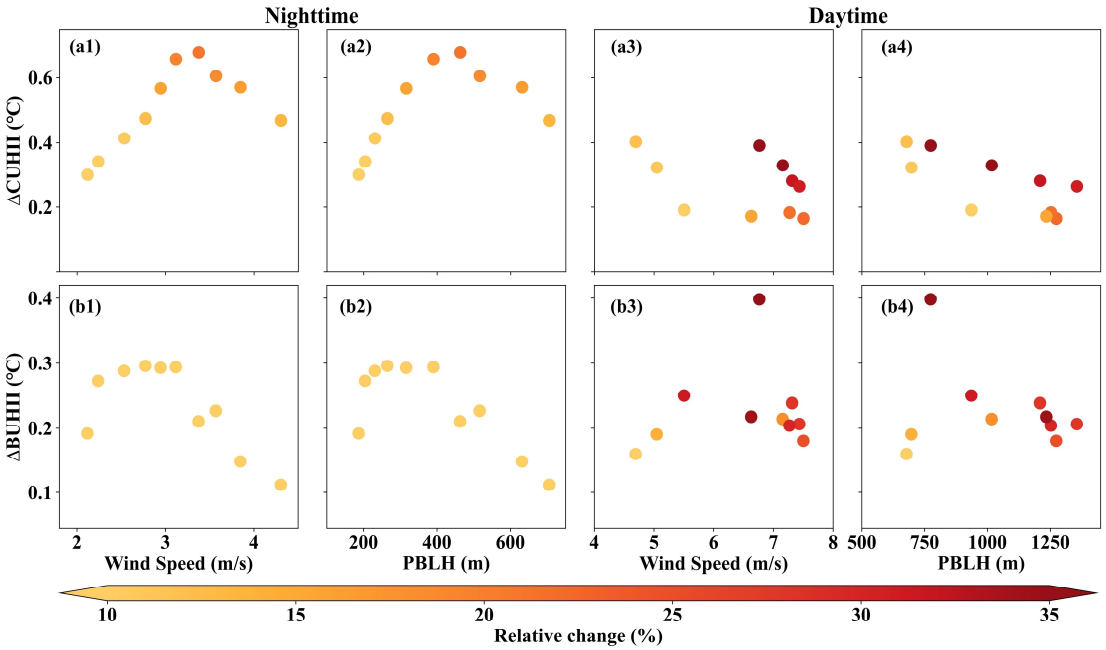

Figure 12. Scatter plots between ΔCUHII and (a1, a3) 10-meter wind speed, and (a2, a4) PBLH between the control simulation and the sensitivity experiment (CTRL minus EXP) over Wuxi (U4) at (a1-a2) nighttime and (a3-a4) daytime. (b1-b4) Same as (a1-a4), but for ΔBUHII. Colours represent the relative change of CUHII or BUHII. Note that only the moment when the northwest wind prevailed in the ROI was reserved.

In addition, the enhancement of downstream UHI (CUHII and BUHII) is primarily contributed to by UHA, though it is not entirely attributable to this mechanism; it is concurrently modulated by other physical processes. For example, advective transport from upstream urban areas can modify local atmospheric conditions (e.g., ambient humidity, stability), which subsequently influence the thermal environment of the downstream city. Furthermore, changes in the underlying surface will also affect local circulation by thermal (e.g., lake-land breeze circulation) and dynamic (e.g., ventilation) effects, which in turn affect wind and temperature in downstream areas. Ultimately, the increase in downstream UHI is a combined result of multiple processes."

We sincerely appreciate your thorough review and hope these revisions meet with your approval.

Once again, thank you very much for your comments and suggestions.

References (For RESPONSE and newly added references in the manuscript):

Avisar, D., Pelta, R., Chudnovsky, A., and Rostkier-Edelstein, D.: High Resolution WRF Simulations for the Tel-Aviv Metropolitan Area Reveal the Urban Fingerprint in the Sea-Breeze Hodograph, JGR Atmospheres, 126, e2020JD033691, https://doi.org/10.1029/2020JD033691, 2021.

Baklanov, A., Molina, L. T., and Gauss, M.: Megacities, air quality and climate, Atmospheric Environment, 126, 235–249, https://doi.org/10.1016/j.atmosenv.2015.11.059, 2016.

Cosgrove, A. and Berkelhammer, M.: Downwind footprint of an urban heat island on air and lake temperatures, npj Clim Atmos Sci, 1, 46, https://doi.org/10.1038/s41612-018-0055-3, 2018.

Guo, J., Zhang, J., Yang, K., Liao, H., Zhang, S., Huang, K., Lv, Y., Shao, J., Yu, T., Tong, B., Li, J., Su, T., Yim, S. H. L., Stoffelen, A., Zhai, P., and Xu, X.: Investigation of near-global daytime boundary layer height using high-resolution radiosondes: first results and comparison with ERA5, MERRA-2, JRA-55, and NCEP-2 reanalyses, Atmos. Chem. Phys., 21, 17079–17097, https://doi.org/10.5194/acp-21-17079-2021, 2021.

Guo, J., Zhang, J., Shao, J., Chen, T., Bai, K., Sun, Y., Li, N., Wu, J., Li, R., Li, J., Guo, Q., Cohen, J. B., Zhai, P., Xu, X., and Hu, F.: A merged continental planetary boundary layer height dataset based on high-resolution radiosonde measurements, ERA5 reanalysis, and GLDAS, Earth Syst. Sci. Data, 16, 1–14, https://doi.org/10.5194/essd-16-1-2024, 2024.

Haeffelin, M., Ribaud, J.-F., Céspedes, J., Dupont, J.-C., Lemonsu, A., Masson, V., Nagel, T., and Kotthaus, S.: Impact of boundary layer stability on urban park cooling effect intensity, Atmos. Chem. Phys., 24, 14101–14122, https://doi.org/10.5194/acp-24-14101-2024, 2024.

Hong, S.-Y., Noh, Y., and Dudhia, J.: A New Vertical Diffusion Package with an Explicit Treatment of Entrainment Processes, Monthly Weather Review, 134, 2318–2341, https://doi.org/10.1175/MWR3199.1, 2006.

Liao, W., Li, Y., Liu, X., Wang, Y., Che, Y., Shao, L., Chen, G., Yuan, H., Zhang, N., and Chen, F.: GloUCP: a global 1 km spatially continuous urban canopy parameters for the WRF model, Earth Syst. Sci. Data, 17, 2535–2551, https://doi.org/10.5194/essd-17-2535-2025, 2025.

Oke, T. R., Mills, G., Christen, A., and Voogt, J. A.: Urban Climates, 1st ed., Cambridge University Press, https://doi.org/10.1017/9781139016476, 2017.

Saha, S., Sharma, S., Kumar, K. N., Kumar, P., Lal, S., and Kamat, D.: Investigation of Atmospheric Boundary Layer characteristics using Ceilometer Lidar, COSMIC GPS RO satellite, Radiosonde and ERA-5 reanalysis dataset over Western Indian Region, Atmospheric Research, 268, 105999, https://doi.org/10.1016/j.atmosres.2021.105999, 2022.

Salamanca, F., Krpo, A., Martilli, A., and Clappier, A.: A new building energy model coupled with an urban canopy parameterization for urban climate simulations—part I. formulation, verification, and sensitivity analysis of the model, Theor Appl Climatol, 99, 331–344, https://doi.org/10.1007/s00704-009-0142-9, 2010.

Sun, Y., Zhang, N., Miao, S., Kong, F., Zhang, Y., and Li, N.: Urban Morphological Parameters of the Main Cities in China and Their Application in the WRF Model, J Adv Model Earth Syst, 13, e2020MS002382, https://doi.org/10.1029/2020MS002382, 2021.

Wang, L., Fan, S., Hu, F., Miao, S., Yang, A., Li, Y., Liu, J., Liu, C., Chen, S., Ho, H. C., Duan, Z., Gao, Z., and Yang, Y.: Vertical Gradient Variations in Radiation Budget and Heat Fluxes in the Urban Boundary Layer: A Comparison Study Between Polluted and Clean Air Episodes in Beijing During Winter, JGR Atmospheres, 125, e2020JD032478, https://doi.org/10.1029/2020JD032478, 2020.

Xue, J., Zong, L., Yang, Y., Bi, X., Zhang, Y., and Zhao, M.: Diurnal and interannual variations of canopy urban heat island (CUHI) effects over a mountain–valley city with a semi-arid climate, Urban Climate, 48, 101425, https://doi.org/10.1016/j.uclim.2023.101425, 2023.

Yang, Y., Zheng, Z., Yim, S. Y. L., Roth, M., Ren, G., Gao, Z., Wang, T., Li, Q., Shi, C., Ning, G., and Li, Y.: PM $_{2.5}$ Pollution Modulates Wintertime Urban Heat Island Intensity in the Beijing-Tianjin-Hebei Megalopolis, China, Geophysical Research Letters, 47, https://doi.org/10.1029/2019GL084288, 2020.

Yang, Y., Guo, M., Wang, L., Zong, L., Liu, D., Zhang, W., Wang, M., Wan, B., and Guo, Y.: Unevenly spatiotemporal distribution of urban excess warming in coastal Shanghai megacity, China: Roles of geophysical environment, ventilation and sea breezes, Building and Environment, 235, 110180, https://doi.org/10.1016/j.buildenv.2023.110180, 2023.

Yu, M., Chen, X., Yang, J., and Miao, S.: A new perspective on evaluating high-resolution urban climate simulation with urban canopy parameters, Urban Climate, 38, 100919, https://doi.org/10.1016/j.uclim.2021.100919, 2021.

Zhu, D. and Ooka, R.: WRF-based scenario experiment research on urban heat island: A review, Urban Climate, 49, 101512, https://doi.org/10.1016/j.uclim.2023.101512, 2023.